Pulsed Electrodeposition of Two-Dimensional Ag Nanostructures on Au(111)

D. Borissov, R. Tsekov, and W. Freyland*

Institute of Physical Chemistry, University of Karlsruhe, D-76128 Karlsruhe, Germany

Received: March 22, 2006; In Final Form: May 19, 2006

One-step pulsed potential electrodeposition of Ag on Au(111) in the underpotential deposition (UPD) region has been studied in 0.5 mM Ag_2SO_4 + 0.1 M H_2SO_4 aqueous electrolyte at various pulse durations from 0.2 to 500 ms. Evolution of the deposited Ag nanostructures was followed by in situ scanning tunneling microscopy (STM) and by measurement of the respective current transients. At short pulse durations a relatively high number density (4×10^{11} cm^{-2}) of two-dimensional Ag clusters with a narrow size and distance distribution is observed. They exhibit a remarkably high stability characterized by a dissolution potential which lies about 200 mV more anodically than the typical potential of Ag−(1 × 1) monolayer dissolution. To elucidate the underlying nucleation and growth mechanism, two models have been considered: two-dimensional lattice incorporation and a newly developed coupled diffusion−adsorption model. The first one yields a qualitative description of the current transients, whereas the second one is in nearly quantitative agreement with the experimental data. In this model the transformation of a Ag−(3 × 3) into a Ag−(1 × 1) structure indicated in the cyclic voltammogram (peaks at 520 vs 20 mV) is taken into account.

I. Introduction

In recent years, pulsed potentiostatic deposition has been employed to fabricate and tailor nanomaterials with specific properties. This includes nanostructures such as long metal nanowires,[1] thin homogeneous magnetic films,[2] and nanoparticles or nanocrystals with excellent size monodispersity;[3] for a recent review see ref 4. The particular advantage of the pulsed electrodeposition technique is that nucleation and growth can be controlled separately by varying the potential pulse amplitudes and durations. In addition, the technique is fast and inexpensive.

For the examples given above, square wave potential pulses in the overpotential region (OPD) have been used and deposition was studied typically on surfaces with low interfacial energy such as graphite.[5,6] This leads to electrocrystallization of three-dimensional (3D) metal particles under conditions of instantaneous nucleation and diffusion-controlled Vollmer−Weber growth mode.[4] In this investigation, we have focused on pulsed electrodeposition in the underpotential range (UPD) where usually homogeneous monolayer formation is expected by gradually changing the electrode potential. In our experiments we used a high-energy surface Au(111) substrate. Ag UPD has been selected in these studies as here a detailed knowledge of UPD phase formation and transitions in different electrolytes exists.[7−10] So, the main objective of this work is to study 2D phase formation and growth of Ag on Au(111) under pulsed electrodeposition conditions in comparison with conventional UPD. The evolution of the 2D nanostructures as a function of time and potential has been followed by in situ STM imaging.

II. Experimental Section

Pulsed electrodeposition in the UPD region of 0.5 mM Ag_2SO_4 (p.a, Merck, Germany) solution on Au(111) in 0.1 M H_2SO_4 (p.a, Merck, Germany) sulfuric aqueous electrolyte was carried out by switching the electrode potential of the working electrode in a conventional three-electrode electrochemical cell from E1 = 550 mV to E2 = 20 mV vs Ag^+/Ag for a very short time; see Figure 1A. The silver wire of the reference electrode had a diameter of 0.3 mm, and its tip was fixed 1 mm above the working electrode with an area of 0.56 cm^2. The corresponding uncompensated *iR* drop we estimate to be 20 mV for current densities of 15 mA/cm^2. The duration of the potential pulse was varied from 0.2 to 500 ms. For these fast measurements, the potentiostat was equipped with a special interface card, ADC750 (AutoLab, Nederlands), which has a maximum conversion speed of 750 kHz and can measure current−time response of the conventional three-electrode electrochemical cell with a shortest interval of 1.3 μs. After one potential pulse from E1 = 550 mV to E2 = 20 mV, the electrochemical cell was switched off and the scanning tunneling microscopy (STM) experiment was performed at the open circuit potential (OCP). In this work, a mechanically polished single-crystal Au(111) was used as a working electrode with a size of 10 mm × 10 mm and a thickness of 2 mm and an orientation misfit of better than 0.1 exhibiting a grain size less than 30 nm (MaTeck, Germany). The following cleaning procedure was employed: First, the crystal was electropolished in 0.1 M H_2SO_4 electrolyte in a conventional electrochemical cell with platinum as a reference and a counter electrode at a constant applied voltage of +4 V for 1 min. Subsequently, the oxide layer was dissolved in 1 M HCl. Then the crystal was thoroughly rinsed with Milli-Q water. To get large monatomic flat terraces, the single-crystal Au(111) was flame annealed in a hydrogen burner to a reddish color for 10 min. Afterward, it was quenched in Milli-Q water, and a droplet of Milli-Q water was left on the gold surface to prevent adsorption of impurities. This procedure resulted in large atomically flat and clean terraces.

In situ STM investigations were carried out with a home-built STM head employed with a 2μ scanner. The STM head was driven by a Molecular Imaging (MI) Pico SPM controller. STM tips used in this work were made of PtIr wire (90%−

* Author to whom correspondence should be addressed. E-mail: Werner.Freyland@chemie.uni-karlsruhe.de.

10.1021/jp061780m CCC: $33.50
Published on Web 07/26/2006

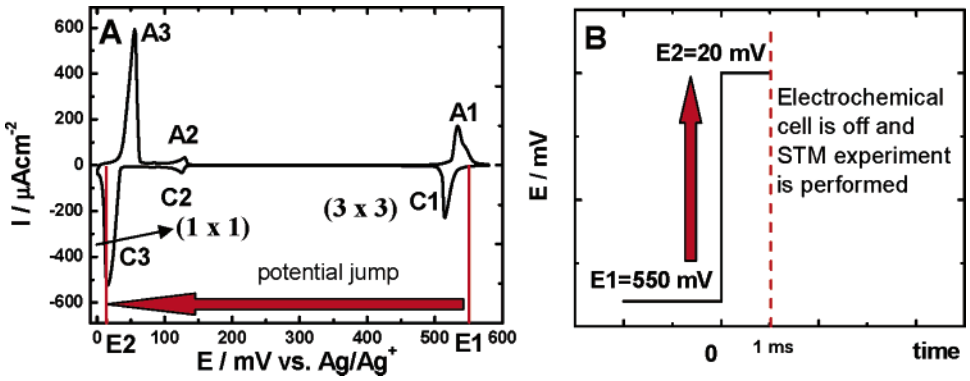

Figure 1. (A) Cyclic voltammogram recorded on single-crystal Au(111) in 0.5 mM Ag_2SO_4 + 0.1 M H_2SO_4 at a sweep rate of 30 mV/s. The arrow shows a potential jump. (B) After one potential pulse from E1 = 550 mV to E2 = 20 mV the electrochemical cell is switched off and STM experiment is performed.

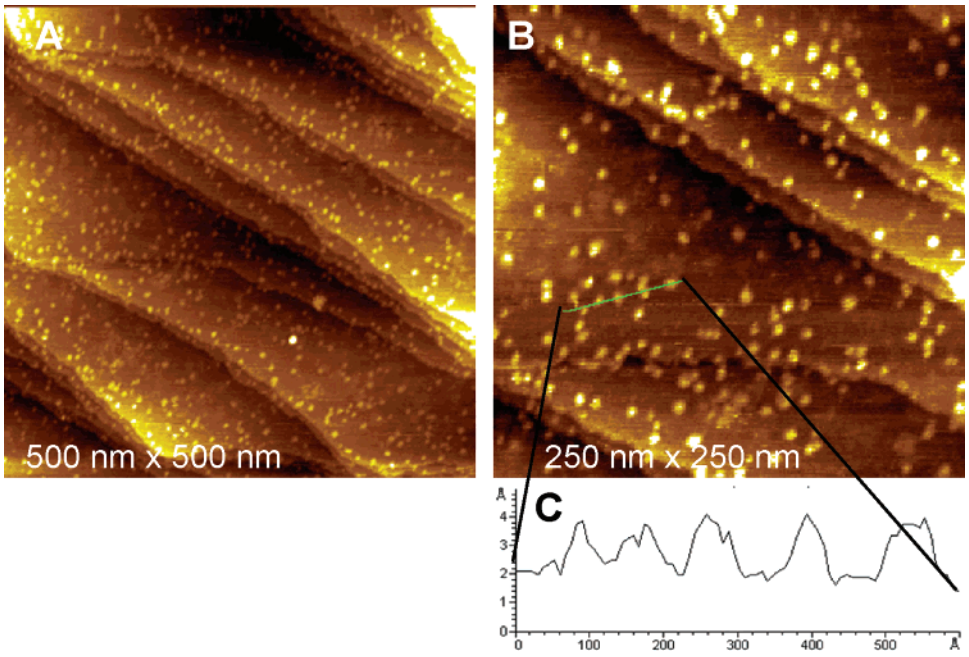

Figure 2. (A) 500 nm × 500 nm in situ STM image of Au(111) after one potential pulse from 550 to 20 mV with a duration of 0.2 ms in 0.5 mM Ag_2SO_4 + 0.1 M H_2SO_4. (B) 250 nm × 250 nm area of the substrate recorded at OCP after 24 h. (C) Cross section analysis of 2D Ag clusters yielding a height of 2 Å.

10% respectively, 0.25 mm in diameter, Advent, England). The tips were produced by electrochemical etching in 4 M NaCN using the "drop-off" method. A PtIr wire, after being washed with ethanol, was vertically anchored to a manipulator and fixed in the middle of a ring wire of Pt acting as a counter electrode. A thin lamella of NaCN solution was formed on the ring electrode crossing the PtIr wire. Then an ac voltage of 4 V was applied between the Pt ring electrode and PtIr wire. Due to the "necking-in" effect, the down part of the wire drops off when its weight exceeds the tensile strength of the necking-in region. Just before dropping the voltage was reduced to 2 V. The down part was caught in a small plastic tip holder so that the apex of the tip was not damaged. For a better control all tips were checked by an optical microscope with 40× magnification before use. To minimize Faradaic currents in STM measurements carried out in the electrolyte, the freshly prepared tips were insulated with an anodic epoxy paint (BASF, ZQ 84-3225 0201, Germany). For this purpose 0.8 cm of PtIr tips were immersed into the epoxy paint and a dc voltage of 25 V was applied for 5 min between the tip (anode) and a counter Pt plate electrode (cathode).

III. Results

After one potential pulse from 550 to 20 mV in 1 mM solution of Ag^+ with a duration of 0.2 ms, the Au(111) surface was examined by in situ STM at OCP. The measured OCP was stabilized at 70 mV. Figure 2A presents an STM image of the surface showing a surprisingly large number of two-dimensional (2D) silver nanoclusters (islands) that have a narrow size distribution suggesting an instantaneous nucleation.

A detailed analysis of the STM images reveals that the 2D Ag nanoclusters are formed all over the surface without any preferential position on the gold terraces or at the step edges. Also, it was found that they have a very high stability because no significant change in their size and spatial distribution was observed for a long span of time; see Figure 2B. A cross section analysis (Figure 2C) reveals silver clusters which have a monatomic height of about 2 Å. To test whether 2D Ag clusters grow under potentiostatic conditions, the electrochemical cell was switched on and the electrode potential was gradually reduced from 70 mV (the actual value of OCP) to 0 mV. From OCP to 30 mV there is no significant change on the surface

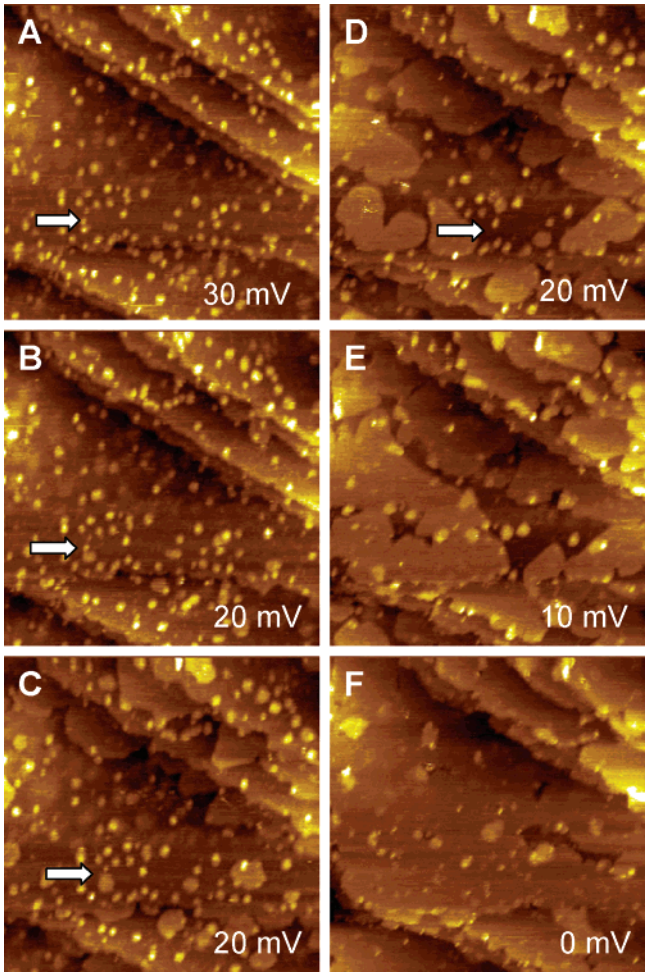

Figure 3. A sequence of in situ STM images after 0.2 ms potential pulse from 550 to 20 mV at various electrode potentials showing the formation of one monolayer of Ag−(1 × 1), size 250 nm × 250 nm: (A) at 30 mV; (B−D) at 20 mV; (E) at 10 mV; (F) at 0 mV. The time span between different images is about 5 min.

(Figure 3A). In accordance with the CV, at 20 mV a new silver phase is being formed at the step edges and at 2D silver clusters as well; see Figure 3B. The development of the island growth was continuously followed at constant applied electrode potential of 20 mV. In Figure 3B−D sequential images are shown with a time interval of about 5 min. The new Ag islands enlarge relatively fast their size and indicate a strong tendency to merge with each other as well as with the existing Ag clusters. Apparently, the silver islands that stem from the pulsed clusters grow with different rates. Approaching the Nernst equilibrium potential, the surface coverage of Ag on Au(111) increases. It is worth noting that almost one monolayer of Ag coverage is reached at 0 mV and the pulsed clusters become almost an unrecognizable part of it (Figure 3F). Interestingly, it seems that before the monolayer of Ag covers the whole surface, some islands are formed on the top of the silver monolayer, perhaps due to the fact that the electrodeposition takes place at or near nonequilibrium conditions. A pseudomorphic (1 × 1) adlayer of Ag is formed that covers and follows the topography of the Au(111) surface.[7−11]

Dissolution of the deposited monolayer of Ag was studied by in situ STM as a function of the applied electrode potential. In Figure 4 STM snapshots are displayed during the dissolution process. It should be noted that although the 2D Ag clusters become a part of the (1 × 1) Ag monolayer, they cannot be

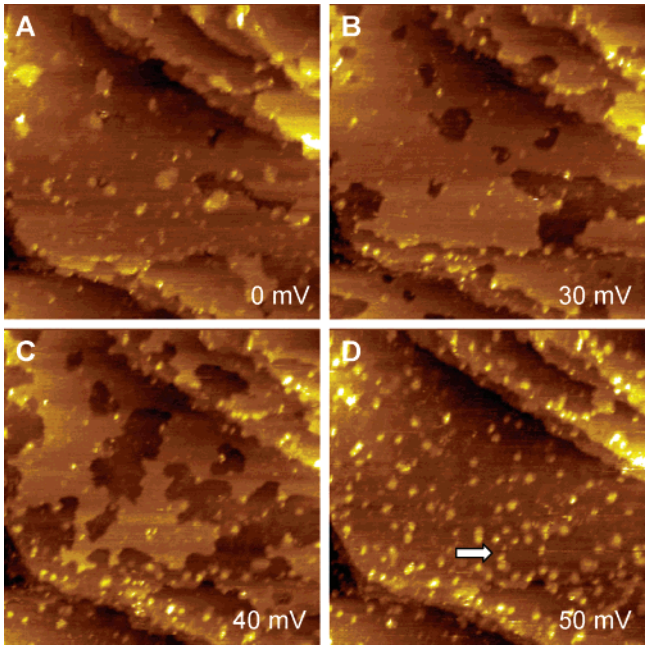

Figure 4. A sequence of STM images showing the dissolution of the Ag−(1 × 1) adlayer, size 250 nm × 250 nm: (A) at 0 mV; (B) at 30 mV; (C) at 40 mV; (D) at 50 mV. The white arrow shows that after dissolution the same 2D pulsed Ag clusters appear on the surface as before (Figure 3) indicating a very high stability.

stripped at positive potentials where usually the (1 × 1)-Ag adlayer is completely dissolved in accordance with the CV (A3 process in the CV). This strongly indicates that the 2D clusters exhibit an anomalous stability. Similar behavior of small Ag and Au nanoclusters on HOPG has already been observed.[12,13] Moreover, a striking result is that some kind of "memory effect" is observed because after dissolution the STM pictures reveal the pulse deposited 2D Ag clusters at the same places on the surface as at the beginning of the deposition; see the white arrows in Figure 4D and Figure 3A. The 2D Ag clusters are evident even at 200 mV as displayed in Figure 5; see the arrows in parts A and B of Figure 5. They start to dissolve slowly in the potential range from 200 to 400 mV; see Figure 4B−D. Possibly, the initial stability of the pulse deposited 2D Ag clusters is due to surface alloying which was observed for this system recently.[7]

The effect of potential pulse duration on the nucleation density and size of 2D Ag clusters has been studied for pulses in the range from 0.2 to 500 ms. Qualitatively, the STM images show that for larger pulse durations the cluster size increases whereas the nucleation density decreases; see Figure 6.

A quantitative analysis of the nearest neighbor distance distribution of 2D Ag clusters is presented in Figure 7 for a pulse experiment of 0.2 ms; see also Figure 2 for the respective STM images. In comparison to a random distribution the experimental histogram is narrower. Distances below 5 nm are missing indicating an average cluster size of 5 nm. The mean nearest neighbor distance is determined to be 10 ± 2 nm, whereas the value of the random distribution is 8.1 nm.[14] The average nucleation density, in this case, is found to be $N_0 = 4 \times 10^{11}$ cm^{-2}.

For the pulsed electrodeposition of Ag on Au(111) in the UPD range, we have recorded the current transients at different pulse durations. Typical results are shown in Figure 8. For short pulses the current decays continuously with time; see the example of a 10 ms pulse time. At larger times a clear bump or

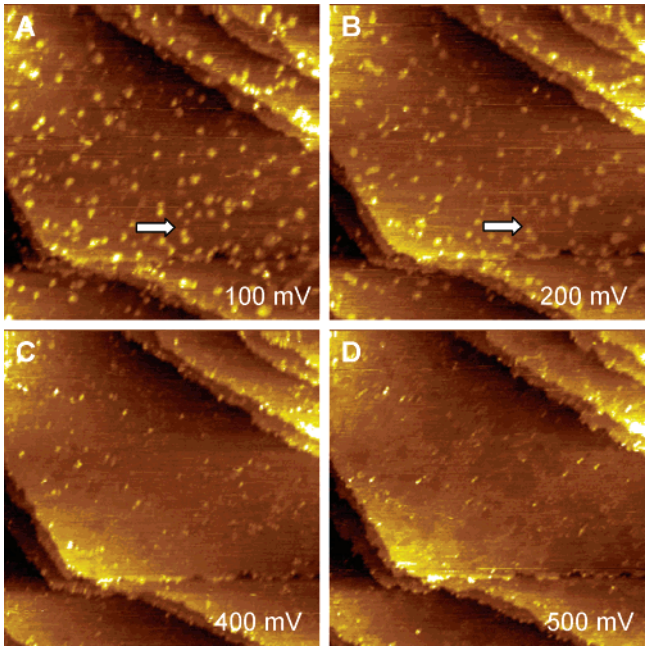

Figure 5. STM images (250 nm × 250 nm) of dissolution of 2D pulsed Ag nanoclusters: (A) at 100 mV the pulse deposited 2D clusters are still visible; (B) at 200 mV the clusters slowly start to dissolve; (C) at 400 mV and (D) at 500 mV they are almost completely dissolved.

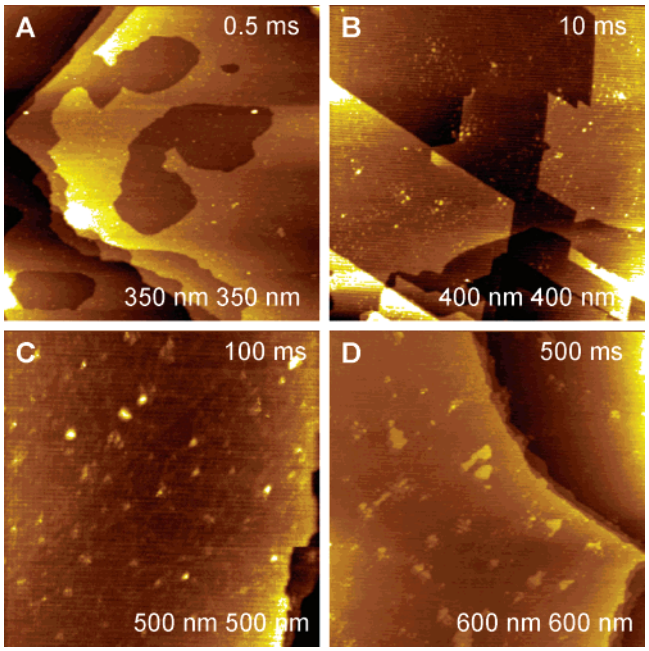

Figure 6. STM images show the effect of pulse duration on cluster size after a potential pulse from 550 to 20 mV: (A) 0.5 ms; (B) 10 ms; (C) 100 ms; (D) 500 ms pulse duration.

maximum is visible at times near 2−3 ms. The strong drop of the current below 1 ms we ascribe to the double layer charging effect; see below.

IV. Discussion

Several features of the STM observations of pulse deposited 2D Ag clusters on Au(111) are worth noting: an unusual stability of clusters on dissolution, the high nucleation density of nearly random distributed clusters, and the peaks in the current transients at short times. To get further insight into the

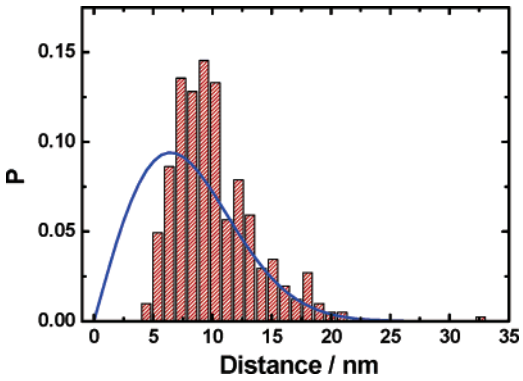

Figure 7. Histogram of distances between nearest neighboring Ag clusters after using a 0.2 ms potential pulse, for STM image; see Figure 2A. The line is drawn according to the Poisson distribution law.[14]

nucleation and growth mechanism of 2D pulsed electrodeposition, in the following we concentrate on the discussion of the current transients. For this aim we consider two simple model descriptions. In the first case we start from standard nucleation models—instantaneous or progressive nucleation—and assume that the rate-determining step of cluster growth is the lattice incorporation of Ag adatoms at the expanding periphery of the nucleation centers. Taking into account double layer charging, the total current−time dependence in the case of instantaneous nucleation is given by (see, e.g., refs 15 and 16)

$$i_{tot}(t) = i_0 \exp(-t/\tau) + p_1 t \exp(-p_2 t^2/2) \qquad (1)$$

where $p_1 = 2\pi F N_0 M k^2 h/\rho$ and $p_2 = 2\pi N_0 M^2 k^2/\rho^2$. Here F is the Faraday constant, N_0 is the initial number density of nuclei, k is the rate constant of lattice incorporation, h is the height of 2D Ag clusters, and M and ρ are the atomic weight and density of a 2D Ag cluster. The time constant of double layer charging is denoted by τ. Figure 9 shows a fit by eq 1 of the current transient measured for a pulse time of 50 ms. The red curve corresponds to instantaneous nucleation, the blue one to progressive nucleation. Both fits are in qualitative agreement with the experimental result whereby the instantaneous nucleation fit gives a better description consistent with the STM observations. The time constant τ is determined to be ∼0.4 ms.

From the fit parameters p_1 and p_2 the following quantities of nucleation and growth model can be derived. The ratio p_1/p_2 yields a charge coverage of about 19 μC/cm^2, which is comparable in magnitude to the charge coverage of the (3 × 3) structure (59 μC/cm^2) occurring at 500 mV but is smaller by roughly a factor of 10 in comparison with (1 × 1) structure (222 μC/cm^2) at 20 mV.[7] Estimating the product N_0k^2 from p_1 yields a value of 1.2 × 10^3 mol^2 s^{-2} cm^{-6}, which is roughly 5 orders of magnitude larger than the corresponding kinetic parameters determined in Cu UPD at near equilibrium conditions.[18] This implies a large rate constant k of the order of 10^{-4} mol s^{-1} cm^{-2} taking for N_0 the above value of 4 × 10^{11} cm^{-2}. In conclusion it is difficult to say how far the simple lattice incorporation model describes the experimental observations.

Since the simple 2D lattice incorporation model does not allow a quantitative description of the measured current transients, we have developed a new model based on coupled diffusion−adsorption kinetics. In brief, the regular diffusion equation has been solved with the following boundary and initial conditions: in the bulk electrolyte, a constant concentration far away from the Au(111) electrode, $c_\infty = c(t,z=\infty)$, is taken,

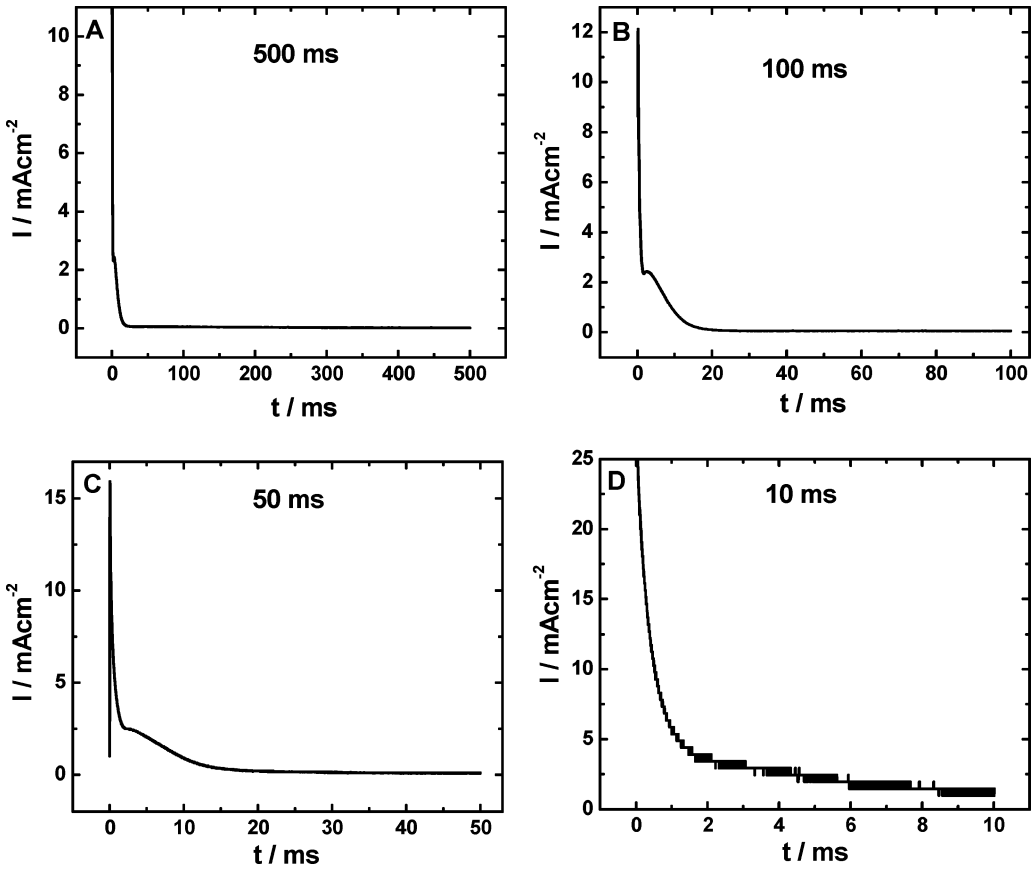

Figure 8. Current−time ($i-t$) responses recorded during the potential pulse from 550 to 20 mV in 0.5 mM Ag_2SO_4 + 0.1 M H_2SO_4 on Au(111) at different pulse durations.

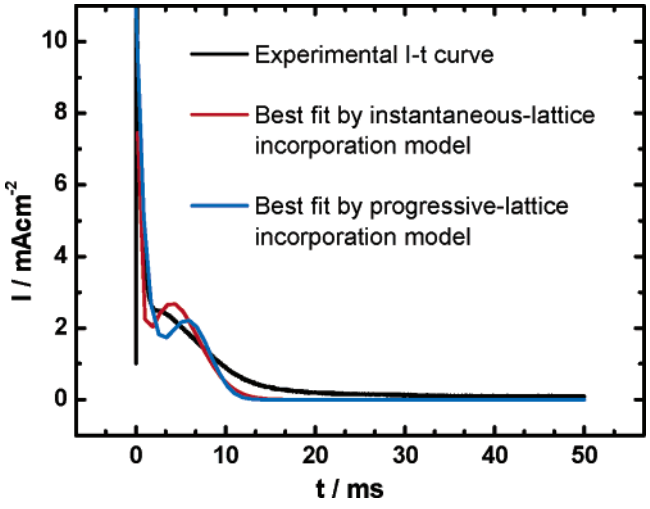

Figure 9. Best fits of theoretical $i-t$ expressions for instantaneous or progressive nucleation under assumption that the rate-determining step is the lattice incorporation of Ag adatoms at the expanding periphery of the nucleation centers.

whereas at the electrolyte/Au(111) interface the diffusion and adsorption fluxes are equal, i.e., $D(\partial_z c)_{z=0} = \partial_t \Gamma$; here D is the bulk diffusion coefficient and Γ is the adsorption of Ag atoms; the initial conditions are constant concentration everywhere in the bulk $c(t=0,z) = c_\infty$ and a bare Au surface $\Gamma(t=0) = 0$ at the beginning of the process. Hence the local concentration is given by the following Laplace image $\tilde{c}(s,z)$ (see, e.g., ref 18)

$$\tilde{c} = c_\infty/s - \tilde{\Gamma}\sqrt{s/D}\,\exp(-\sqrt{s/D}z) \qquad (2)$$

Further analysis requires modeling of the adsorption kinetics. From the STM and experimental CV results it is clear that the Ag atoms can form two different stable surface phases on the Au surface: the Ag−(3 × 3) phase occurring at 520 mV and the Ag−(1 × 1) at 20 mV; see also ref 7. Let us denote the dilute one as the α-phase and the condensed one as the β-phase. If the electrode potential changes continuously, the α-phase appears at about 520 mV and then it is transformed into the β-phase at around 20 mV. However, in contrast to quasi-equilibrium electrodeposition, if the potential jumps from 550 mV directly to 20 mV, there is no α-phase at the beginning and, hence, the formation of the two phases will take place simultaneously. It is conceivable, that the creation of the β-phase requires first the presence of the α-phase. Thus, a linearized kinetic model of the adsorption of Ag on Au electrode after the potential jump reads

$$\partial_t \Gamma_\alpha = k_a c_s(\Gamma_\alpha^\infty - \Gamma_\alpha) \approx k_\alpha \Gamma_\alpha^\infty c_s - k_a c_\infty \Gamma_\alpha \qquad (3)$$

$$\partial_t \Gamma_{\beta-\alpha} = k_t \Gamma_\alpha c_s(\Gamma_{\beta-\alpha}^\infty - \Gamma_{\beta-\alpha}) \approx k_t c_\infty \Gamma_{\beta-\alpha}^\infty \Gamma_\alpha - k_t c_\infty \Gamma_\alpha^\infty \Gamma_{\beta-\alpha} \qquad (4)$$

where Γ_α is the number of atoms per unit area forming the α-phase, $\Gamma_{\beta-\alpha}$ is the number of atoms per unit area added between the atoms of the dilute α-phase to convert it into the denser β-phase, and Γ_α^∞ and $\Gamma_{\beta-\alpha}^\infty$ represent the saturation coverages, $c_s = c(t,z=0)$ is the subsurface concentration, k_α is the adsorption constant, and k_t is the rate constant of transformation of α- into β-phase. Note, that desorption is completely neglected in eqs 3 and 4. Solving these equations by Laplace

transformation yields the following Laplace images of the adsorptions

$$\tilde{\Gamma}_\alpha = k_a \Gamma_\alpha^\infty \tilde{c}_s/(s + k_a c_\infty) \quad (5)$$

$$\tilde{\Gamma}_{\beta-\alpha} = k_t c_\infty \Gamma_{\beta-\alpha}^\infty k_a \Gamma_\alpha^\infty \tilde{c}_s/(s + k_a c_\infty)(s + k_t c_\infty \Gamma_\alpha^\infty) \quad (6)$$

The total adsorption of Ag atoms on the Au surface is a sum of the partial adsorptions above, i.e.

$$\tilde{\Gamma} = \tilde{\Gamma}_\alpha + \tilde{\Gamma}_{\beta-\alpha} = k_a \Gamma_\alpha^\infty \tilde{c}_s \frac{s + k_t c_\infty (\Gamma_\alpha^\infty + \Gamma_{\beta-\alpha}^\infty)}{(s + k_a c_\infty)(s + k_t c_\infty \Gamma_{\beta-\alpha}^\infty)} \quad (7)$$

Introducing eq 7 in eq 2 leads to an expression for the Laplace image of the local concentration. Using it one can derive the Laplace image of the subsurface concentration in the form

$$\tilde{c}_s = c_\infty \frac{(s + k_a c_\infty)(s + k_t c_\infty \Gamma_\alpha^\infty)}{s[(s + k_a c_\infty \Gamma_\alpha^\infty) + k_a \Gamma_\alpha^\infty (s + k_t c_\infty \Gamma_\alpha^\infty + k_t c_\infty \Gamma_{\beta-\alpha}^\infty)\sqrt{s/D}]} \quad (8)$$

which depends on both the diffusion in the bulk and the kinetics of adsorption. Finally, the measured electric current is a sum of the electric current due to Ag deposition and the current due to the charging of the electric double layer

$$\tilde{i} = Fs\tilde{\Gamma} + A/(s + 1/\tau) \quad (9)$$

Here A is a constant and τ is the time constant of the double layer charging. Substituting $\tilde{c}_s$ from eq 8 and introducing the result of $\tilde{\Gamma}$ in eq 9 leads to the following expression for the Laplace image of the current

$$\tilde{i} = \frac{Fk_a c_\infty \Gamma_\alpha^\infty (s + k_t c_\infty \Gamma_\alpha^\infty + k_t c_\infty \Gamma_{\beta-\alpha}^\infty)}{(s + k_a c_\infty)(s + k_t c_\infty \Gamma_\alpha^\infty) + k_a \Gamma_\alpha^\infty (s + k_t c_\infty \Gamma_\alpha^\infty + k_t c_\infty \Gamma_{\beta-\alpha}^\infty)\sqrt{s/D}} + \frac{i_0 - Fk_a c_\infty \Gamma_\alpha^\infty}{s + 1/\tau} \quad (10)$$

where the constant A is expressed by the initial current $i_0 = i(t=0)$. The analytical inversion of the Laplace image from eq 10 is impossible. For this reason numerical calculations have been employed. Some of the parameters in eq 10 are known: $c_\infty = 1$ mM, $D = 1.65 \times 10^{-5}$ cm^2/s,[19] and $\tau = 0.4$ ms. From our previous investigations[7] we conclude that the α-phase corresponds to 0.25 ML, while the condensed phase (β-phase) forms a complete monolayer. Thus, one can estimate that the maximal adsorptions are equal to $\Gamma_\alpha^\infty = 0.25 N_A/\pi d^2 = 1.6$ μmol/m^2 and $\Gamma_{\beta-\alpha}^\infty = 0.75 N_A/\pi d^2 = 4.8$ μmol/m^2, where $d = 2.89$ Å is the distance between the surface Au atoms. Because of the high electrolyte concentration, the relaxation of the double layer is very fast, on the order of 1 ms. For the initial current, we adopt the value of $i_0 = 16$ mA/cm^2 in accordance with Figure 8C. The remaining other two parameters are determined by a fit of the dependence i vs t for the 50 ms pulse experiment; see Figure 8C. For this purpose, the inverse Laplace transformation of eq 10 was performed numerically and then fitted to the experimental i vs t for 50 ms pulse data varying the constants k_a and k_t. The best fit corresponds to $k_a c_\infty = 0.1$ ms^{-1} and $k_t c_\infty \Gamma_{\beta-\alpha}^\infty = 1$ ms^{-1}. The theoretical dependence of the $i-t$ response for a 50 ms potential pulse as calculated from eq 10 is plotted in Figure 10. As is seen the theory reproduces very well the characteristic maximum at about 2 ms after the double layer charging. Obviously, this model gives a better fit to the experimental data than the simple lattice incorporation description, although slight deviations remain in the time interval between 10 and 20 ms. In Figure 11 the time dependence of the surface concentration, $c_s(t)$, and the adsorption of α- and β-phases, respectively, are plotted. Evidently, at the beginning, the dilute phase (α) forms, which later completely transforms into the condensed one (β). The surface concentration is substantially decreased compared to the bulk one and the slow diffusion kinetics determines the current−time response at larger times. Due to the limitation approximation, the model applies only in the limit of short times and does not describe the evolution of the coverage at longer times.

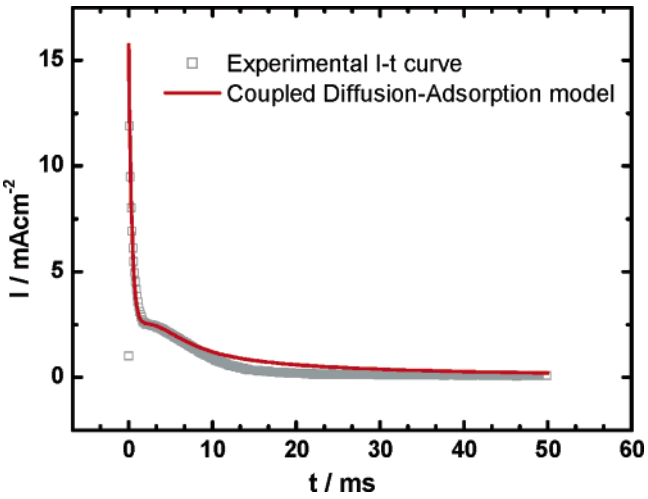

Figure 10. The theoretical dependence of current vs time for a 50 ms potential pulse obtained from the coupled diffusion−adsorption model according to eq 10 in comparison to experimental data points.

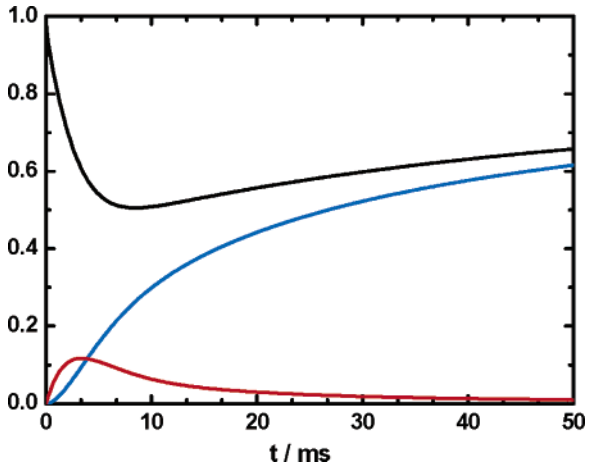

Figure 11. Evolution of the relative subsurface concentration c_s/c_∞ (black line) and the relative coverage by the α-phase $\Gamma_\alpha/\Gamma_\alpha^\infty - \Gamma_{\beta-\alpha}/\Gamma_{\beta-\alpha}^\infty$ (red line) and by the β-phase $\Gamma_{\beta-\alpha}/\Gamma_{\beta-\alpha}^\infty$ (blue line), respectively.

Acknowledgment. We acknowledge financial support by Fonds der Chemischen Industrie.

References and Notes

(1) Walter, E. C.; Murray, B. J.; Favier, F.; Kaltenpoth, G.; Grunze, M.; Penner, R. M. *J. Phys. Chem. B* **2002**, *106*, 11407.

(2) Rastei, M. V.; Colis, S.; Bucher, J. P. *Chem.. Phys. Lett.* **2006**, *417*, 217.

(3) Zoval, J. V.; Lee, J.; Gorer, S.; Penner, R. M. *J. Phys. Chem. B* **1998**, *102*, 1166.
(4) Penner, R. M. *J. Phys. Chem. B* **2002**, *106*, 3339.
(5) Poetzschke, R. T.; Gervasi, C. A.; Vinzelberg, S.; Staikov, G.; Lorenz, W. J. *Electrochim. Acta* **1995**, *40*, 1469−74.
(6) Ertl, G. *Electrochim. Acta* **1998**, *43*, 2743−2750.
(7) Borissov, D.; Aravinda, C. L.; Freyland, W. *J. Phys. Chem. B* **2005**, *109*, 11605.
(8) Esplandiu, M. J.; Schneeweiss, M. A.; Kolb, D. M. *Phys. Chem. Chem. Phys.* **1999**, *1*, 4847.
(9) Garcia, S.; Salinas, D.; Mayer, C.; Schmidt, E.; Staikov, G.; Lorenz, W. J. *Electrochim. Acta* **1998**, *43*, 19.
(10) Chen, C. H.; Vesecky, S. M.; Gewirth, A. A. *J. Am. Chem. Soc.* **1992**, *114*, 451.
(11) Itaya, K. *Nanotechnology* **1992**, *3*, 185.
(12) Ng, K. H.; Liu, H.; Penner, R. M. *Langmuir* **2000**, *16*, 4016.
(13) Boxley, C. J.; White, H. S.; Lister, T. E.; Pinhero, P. J. *Phys. Chem. B* **2003**, *107*, 451.
(14) Milchev, A. *J. Chem. Phys.* **1994**, *100*, 5160.
(15) Greif, R.; Peat, R.; Peter, L. M.; Pletcher, D.; Robinson, J. *Instrumental Methods in Electrochemistry*; Ellis Horwood: New York, 1990.
(16) Scharifkers, B.; Hills, G. *Electrochim. Acta* **1983**, *28*, 879.
(17) Palomar-Pardave, M.; Gonzalez, I.; Batina, N. *J. Phys. Chem. B* **2000**, *104*, 3545.
(18) Bard, A. J.; Faulkner, L. R. *Electrochemical Methods*; Wiley and Sons: New York, 2001.
(19) Lide, D. R.; Ed. *CRC Handbook of Chemistry and Physics*; CRC Press: Boca Raton, FL, 2004.